Numerical study of bluff-body non-premixed flame structures using laminar flamelet model

M Hossain* and **W Malalasekera**
Wolfson School of Mechanical and Manufacturing Engineering, Loughborough University, Leicestershire UK

The manuscript was received on 27 September 2004 and was accepted after revision for publication on 9 March 2005.

DOI: 10.1243/095765005X28616

Abstract: A laminar flamelet model is applied for bluff-body stabilized flames to study the flow field, mixing pattern, and the flame structure at two different velocities. The $k-\varepsilon$ turbulence model is applied for accounting the turbulence fluctuations. It is found that the recirculation zone dominates the near field, while the far field structure is similar to the jet flow. The intermediate neck zone is the intense mixing region. The computation shows that the fuel jet velocity has significant effect on the structure of the flow field, which in turn has significant effect on the combustion characteristics. The laminar flamelet model is found to be adequate for simulating the temperature and the flame composition inside the recirculation zone. The flamelet model has, however, failed to account for the local extinction in the neck zone. Possible limitation of the laminar flamelet model to predict the local extinction is discussed.

Keywords: laminar flamelet, bluff-body, local extinction

1 INTRODUCTION

The accurate prediction of combustion in practical systems has attracted the attention of many researchers over the last few decades because of its potential impact on the development of improved combustion equipments. Better thermal efficiency and lower pollution emission are two of the benefits that can be obtained from the development of advanced combustion models. Over the years, several combustion models that account for the interaction between turbulence and chemistry have been developed and applied to a number of flames ranging from simple jet flames to complex combustion chambers. Non-premixed combustion models that are currently available are conserved scalar-based flame sheet model [**1**], eddy break-up and eddy dissipation model [**2**, **3**], laminar flamelet model [**4**, **5**], conditional moment closure (CMC) model [**6**], and probability density function (pdf) transport model [**7**, **8**]. Last three models are regarded as advanced models capable of handling the finite-rate chemistry or nonequilibrium chemistry effects. The pdf transport model is theoretically the most accurate and is capable of handling the reaction rate term without any modelling assumption. However, the model is very resource-intensive and the application of the model for industrial calculations is still not widespread. The CMC model is a newer model and currently gaining some success in jet flames [**9**]. However, the model is again resource intensive and its successful application in practical situations is yet to be assessed. The flame sheet and eddy break-up models are currently the viable option for industrial applications and these models have been incorporated in a number of commercial CFD codes including FLUENT and CFX. Coelho and Peters [**10**, **11**] have reported successful incorporation of the laminar flamelet model into a commercial CFD code through the user subroutine for simulating an industrial combustor.

The steady laminar flamelet model assumes a turbulent flame as an ensemble of laminar flamelets embedded in the turbulent flame, which are continuously stretched by the turbulent field [**4**, **5**]. The laminar flamelets are usually obtained from the numerical computation of one-dimensional laminar counterflow diffusion combustion. The flamelet structures are then linked with the turbulent flame

Corresponding author: Walfson School of Mechanical Manufacturing Engineering, Loughborough University, Loughborough, Leicestershire LE11 3TU, UK.

through the scalar dissipation rate. The scalar dissipation rate acts as the parameter to include finite-rate chemistry effects in the turbulent combustion. In theory, the laminar flamelet model is capable of prediction of local extinction [**12**, **13**]. If the scalar dissipation rate exceeds a critical value, the extinction limit, the flame is quenched and the flamelet is represented by a pure mixing flamelet. This model has been used by Sanders and Lamers [**14**] to predict the lift-off height of a jet flame. However, the strain rate, rather than the scalar dissipation was used as the non-equilibrium parameter to obtain the correct scaling behaviour. Bray and Peters [**15**] also used a modified scalar dissipation rate to obtain the correct scaling for the lift-off height. However, Hossain [**16**] has shown that the strain rate or the modified scalar dissipation rate is not capable of reproducing temperature and mass fraction of major and minor species. Gran *et al.* [**13**] showed that laminar flamelet model with two flamelet libraries, one for burning flamelet and one for extinguished flamelet, could predict the local extinction. However, the experimental data used for the validation of the model were rather limited. It is, therefore, essential that the existing laminar flamelet model be assessed against a large number of nonintrusive, spontaneous measurements at different conditions before the predictive quality can be confidently implemented for design purposes. In previously published work, the present authors reported the application of the laminar flamelet model for NO formation [**17**] and the development of a novel model for including radiation heat transfer into the laminar flamelet model [**18**]. In the present study, the application of the laminar flamelet model is extended to a flame with higher velocity, which shows considerable local extinction.

The experimental data on bluff-body CH_4/H_2 (1:1 by volume) flames of Dally *et al.* [**19**] are used for the numerical investigation in the present study. Dally *et al.* [**19**] have provided a comprehensive set of experimental data with different fuel jet velocities exhibiting different level of local extinction. The flames are designated as HM1 to HM3 depending on fuel jet velocity. The HM1 has a jet velocity of 118 m/s and does not show local extinction. The HM3 flame with 214 m/s fuel velocity shows considerable local extinction. The HM1 was designated as a standard test case for validating advanced combustion models by the 'International Workshop on Measurements and Computations of Turbulent Nonpremixed Flames (TNF)' (http://www.ca.sandia.gov/tnf/abstract.html). The HM1 flame has been investigated numerically by different researchers in both the 3rd and 5th TNF workshop. The HM3 flame has not been investigated till now. The objective of the present study is to apply the laminar flamelet model to model both HM1 and HM3 flames to ascertain its ability to calculate flames under different level of non-equilibrium effects.

2 MATHEMATICAL MODEL

The numerical model of turbulent combustion is formulated from the Favre-averaged Navier–Stokes equations together with turbulence and combustion models. Farve-averaged Navier–Stokes equations can be expressed in Cartesian tensor notation as

$$\frac{\partial \bar{\rho}\tilde{u}_j}{\partial x_j} = 0 \tag{1}$$

$$\frac{\partial}{\partial x_j}\left(\bar{\rho}\tilde{u}_j\tilde{u}_i\right) = -\frac{\partial P}{\partial x_i} + \mu_{\text{eff}}\frac{\partial}{\partial x_j}\left(\frac{\partial u_j}{\partial x_i} + \frac{\partial u_i}{\partial x_j}\right) \tag{2}$$

where μ_{eff} is the effective viscosity given by $\mu_{\text{eff}} = \mu + \mu_{\text{t}}$.

The eddy viscosity μ_{t} is given by

$$\mu_{\text{t}} = \bar{\rho}C_\mu\frac{\tilde{k}^2}{\tilde{\varepsilon}}$$

In the present study, the $k-\varepsilon$ turbulence model is used for accounting the turbulence fluctuations in the flow field. The equation used to model turbulence kinetic energy, k, is of the form

$$\frac{\partial}{\partial x_j}(\bar{\rho}\tilde{u}_j\tilde{k}) = \frac{\partial}{\partial x_j}\left(\frac{\mu_{\text{t}}}{\sigma_k}\frac{\partial \tilde{k}}{\partial x_j}\right) + G - \varepsilon \tag{3}$$

where G is turbulence production due to strain and is given by

$$G = \mu_{\text{t}}\left(\frac{\partial \tilde{u}_i}{\partial x_j} + \frac{\partial \tilde{u}_j}{\partial x_i}\right)\frac{\partial \tilde{u}_i}{\partial x_j}$$

The transports equation for the dissipation of turbulent kinetic energy ε is of the form

$$\frac{\partial}{\partial x_j}(\bar{\rho}\tilde{u}_j\tilde{\varepsilon}) = \frac{\partial}{\partial x_j}\left(\frac{\mu_{\text{t}}}{\sigma_\varepsilon}\frac{\partial \tilde{\varepsilon}}{\partial x_j}\right) + C_{\varepsilon 1}\frac{\tilde{\varepsilon}}{\tilde{k}}G - C_{\varepsilon 2}\bar{\rho}\frac{\tilde{\varepsilon}^2}{\tilde{k}} \tag{4}$$

The model constants C_μ, $C_{\varepsilon 1}$, $C_{\varepsilon 2}$, σ_k, σ_ε have the values 0.09, 1.60, 1.92, 1.3, and 1.0, respectively. The value of $C_{\varepsilon 1}$ is modified from the standard value of 1.44 to 1.60 in order to reduce the spreading rate of the fuel jet following the work of Dally *et al.* [**20**] and Hossain *et al.* [**18**]. The value of $C_{\varepsilon 1} = 1.60$ is also recommended for bluff-body flames by the 'International Workshop on Measurements and Computations of Turbulent Nonpremixed Flames (TNF)' (http://www.ca.sandia.gov/tnf/abstract.html).

2.1 Laminar flamelet model

The laminar flamelet model views the turbulent flame as an ensemble of laminar flamelet structures, which are corrugated by the action of turbulent fluctuations [**4**, **5**]. The laminar flamelet modelling of turbulent combustion is a two-step process. In the first step, a laminar flamelet library is calculated by solving governing equations for a one-dimensional laminar counterflow diffusion flame. A detailed chemical reaction mechanism and a realistic transport properties can be prescribed for calculating the flamelet library as the flow is laminar. In the second step, the flamelet profiles are used as an input data set to a CFD code, which calculates the mean scalar variables in a turbulent combustion.

The flamelet profiles specify temperature, density, and species concentrations by the mixture fraction and the scalar dissipation rate. For turbulent flames, the mean scalar variables are computed from the laminar flamelet relationship of mixture fraction and scalar dissipation rate by integrating over a joint probability density function as

$$\tilde{\phi} = \int_0^\infty \int_0^1 \phi(Z,\chi) P(Z,\chi)\, \mathrm{d}Z\, \mathrm{d}\chi \tag{5}$$

The assumption of statistical independence leads to $P(Z,\chi) = P(Z)P(\chi)$ [**4**]. The probability density function $P(Z)$ is assumed as a beta distribution and the $P(Z)$ is constructed from transport equations of mean mixture fraction, $\tilde{Z}$, and mixture fraction variance, $\tilde{Z}''^2$

$$\frac{\partial}{\partial x_j}(\bar{\rho}\tilde{u}_j\tilde{Z}) = \frac{\partial}{\partial x_j}\left(\frac{\mu_\mathrm{t}}{\sigma_\mathrm{t}}\frac{\partial \tilde{Z}}{\partial x_j}\right) \tag{6}$$

$$\frac{\partial}{\partial x_j}(\bar{\rho}\tilde{u}_j\tilde{Z}''^2) = \frac{\partial}{\partial x_j}\left(\frac{\mu_\mathrm{t}}{\sigma_\mathrm{t}}\frac{\partial \tilde{Z}''^2}{\partial x_j}\right) + C_{g1}\mu_\mathrm{t}\left(\frac{\partial \tilde{Z}''^2}{\partial x_j}\right)^2 - C_{g2}\frac{\tilde{\varepsilon}}{\tilde{k}}\bar{\rho}\tilde{Z}''^2 \tag{7}$$

where $\sigma_\mathrm{t} = 0.7$ and the constants $C_{g1} = 2.8$ and $C_{g2} = 2.0$.

In the CFD code, transport equations are solved for the mean mixture fraction $\tilde{Z}$ and mixture fraction variance $\tilde{Z}''^2$. The mean and variance of the mixture fraction completely describe the beta function.

The mean value of the scalar dissipation rate can be modelled as

$$\tilde{\chi} = C_\chi \frac{\tilde{\varepsilon}}{\tilde{k}}\tilde{Z}''^2 \tag{8}$$

where $\tilde{k}$ and $\tilde{\varepsilon}$ are the mean turbulence kinetic energy and energy dissipation rate, respectively and C_χ is a constant set equal to 2.0 [**4**]. The distribution of the scalar dissipation rate, $P(\chi)$, is assumed to be log-normal [**4**]. The standard deviation for the log-normal distribution of the scalar dissipation rate is set equal to $\sigma_\chi^2 = 2.0$ [**4**].

3 PROBLEM CONSIDERATION

3.1 Experimental configuration

The bluff-body flames experimentally studied and reported by Dally *et al.* [**19**] are used for the numerical investigation of the present study. Dally *et al.* [**19**] reported a detailed experimental study for a number of fuels with different inlet velocities. The CH_4/H_2 (1:1 by volume) fuel is selected for the present study with inlet velocity of 118 m/s and 214 m/s. The flames are designated as HM1 and HM3, respectively. The coflow air velocity was set at 40 m/s for both the fuel jet velocity cases. The schematic drawing of the bluff-body stabilized flame is shown in Fig. 1. The bluff-body burner has an outer diameter of 50 mm and a concentric jet diameter of 3.6 mm. The burner is placed in a wind tunnel of 254 mm × 254 mm cross-section.

3.2 Computational details

An existing finite volume in-house CFD code is used for solving the governing differential equations and is modified to include the laminar flamelet model. The laminar flamelet model requires a library of flamelets as an input. The flamelet library is generated from the simulation of one-dimensional laminar counterflow diffusion flame using RUN-1DL code [**21**]. The one-dimensional counterflow diffusion flame calculation provides flamelet profiles in the physical space, which are then converted into the mixture fraction space by using Bilger formula for mixture fraction [**22**]. The chemical mechanism used to generate flamelet profiles comprises 16 species and 40 reaction steps. The reaction mechanism is known as Warnatz's mechanism and is taken from the reference [**23**]. During the one-dimensional laminar counterflow diffusion flame calculation, the differences in molecular diffusivities and hence, nonunity Lewis number are generally included. However, in the present study, the molecular diffusion of the species is set according to the unity Lewis number assumption. This is because in turbulent flames the diffusion of individual species depends on the turbulent diffusion rather than the molecular diffusion. Dally *et al.* [**19**] have shown that there is little or no differential diffusion effects in the HM1 and HM3

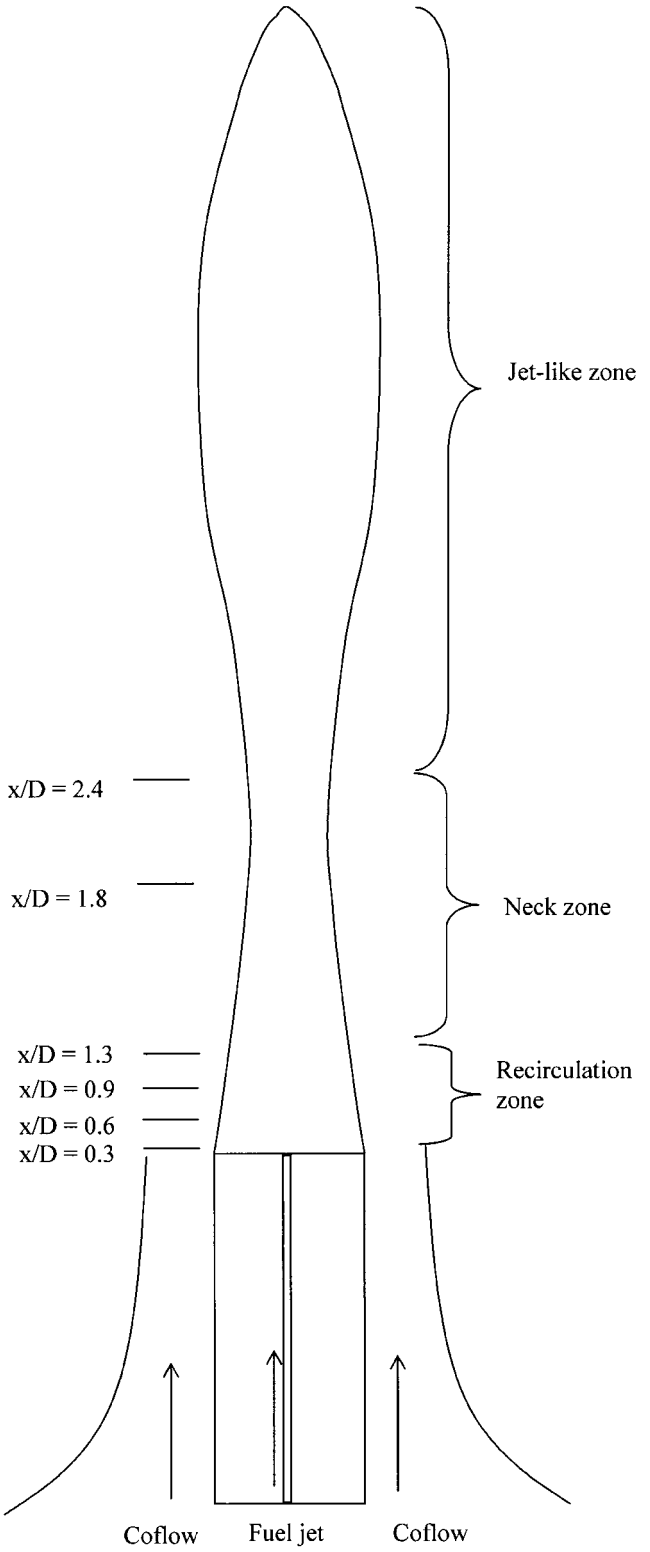

Fig. 1 Schematic drawing of a bluff-body and measuring locations

flames. Accordingly, it is much more realistic to compare turbulent flame composition with those flamelets computed with the unity Lewis number assumption. Hossain and Malalasekera [**17**] have also reported that the unity Lewis number provides better representation of the molecular diffusion of the species for this flame. The flamelet library comprises seven libraries for the scalar dissipation rate of 0.06, 0.43, 2.14, 10.69, 21.31, 38.50/s (extinction limit) and an extinguished flamelet represented by the pure mixing or air and fuel.

The 2D axisymmetric computational domain extends 170 mm in the radial direction and 216 mm in the arial direction. A 99 (axial) $\times$ 89 (radial) grid arrangement is used in the calculation. This grid arrangement was previously shown by the authors to provide grid independent solution of this bluff-body geometry [**18**]. A fully developed velocity was specified at the inlet.

4 RESULTS AND DISCUSSIONS

4.1 Flow field and flame structure

Bluff-body flames are characterized by three distinct zones: (1) the recirculation zone, (2) the neck zone, and (3) the jet like structure. Figure 2 shows the computed streamlines for the velocity of 118 and 214 m/s, showing different zones. The recirculation zone extends up to $x/D = 1.0$ downstream of the face of the burner. Two vortices are observed inside the recirculation zone for the case of 118 m/s fuel jet velocity. The outer vortex is on the face of

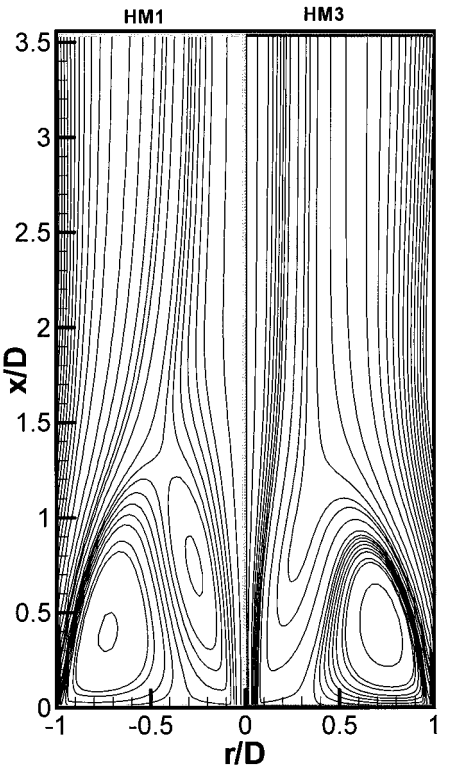

Fig. 2 Contour plots of computed streamlines

the bluff-body and is bigger. The inner vortex lies further downstream and is much narrower. Two shear layers are also observed inside the recirculation zone. The first is the inner layer between the fuel jet and the inner vortex; the second one is the outer layer between the outer edge of the outer vortex and the coflow. With the increase of the jet velocity to 214 m/s, the jet expands and drags the inner vortex with it. The inner vortex loses its recirculation pattern and becomes part of the jet. At the same time, the outer vortex becomes shorter and smaller. Downstream of the recirculation zone is the neck zone, where intense mixing takes place. This is an ideal region to validate the combustion models for the turbulence–chemistry interaction, because the intense mixing of fuel and air leads to non-equilibrium effects in this region. Further downstream, the flow expands in a jet-like manner.

Figure 3 shows the computed mixture fraction contours at different velocities. For the HM1 flame with the jet velocity of 118 m/s, the stoichiometric mixture fraction ($Z = Z_{st} = 0.05$) lies outside the outer edge of the outer vortex. The mixture strength inside the outer vortex is fuel rich and uniform near the face of the burner. The inner vortex contains non-uniform fuel rich mixture. With the increase of the jet velocity to 214 m/s in the HM3 flame, the stoichiometric mixture fraction lines move closer to the fuel jet and lie outside the inner edge of the outer vortex. The core of the vortex becomes fuel lean.

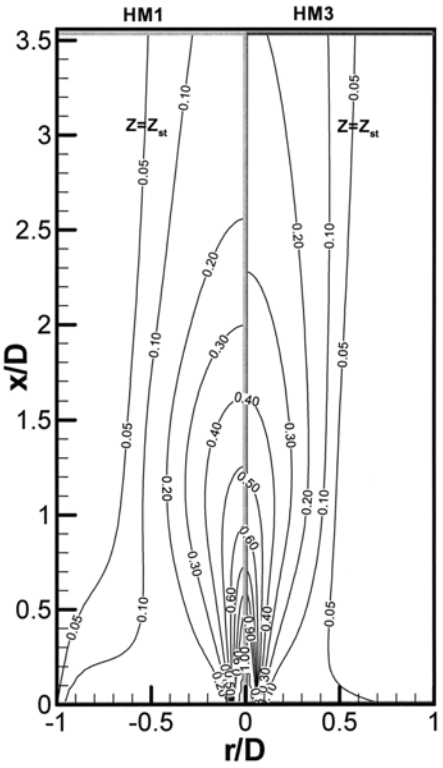

Fig. 3 Contour plots of computed mixture fraction

From the computational results it is apparent that the momentum flux of the jet influences the structure of the recirculation zone. The momentum flux also influences the location of the stoichiometric mixture fraction or the flame front. This then leads to the different flame structure inside the recirculation zone.

4.2 Compositional structure

The comparison of the experimental measurements and the predictions for the two different flames are reported in this section. Figure 4 shows the radial profiles of mixture fraction at different locations. The agreement between the prediction and measurement is very good inside the recirculation zone ($x/D < 1.0$) for both flames. In the neck zone, the agreement is better for the HM3 flame, whereas there is underprediction for the HM1 flame. This underprediction can be attributed to the shortcoming of the $k - \varepsilon$ model, which is known to overpredict the decay rate of the jet. The use of $C_{\varepsilon 1} = 1.60$ has improved the prediction for the HM3 flame, but was not found to be adequate for the HM1 flame.

Radial profiles of the mixture fraction variance are shown in Fig. 5. At $x/D = 0.26$, two peaks are observed in the profiles of both flames. These peaks represent the location of the shear layer. The peak at the outer shear layer is well predicted for both flames; however, the peak in the inner shear layer is overpredicted. Further downstream (at $x/D = 0.6$ and $x/D = 0.9$), three peaks are observed in the mixture fraction variance profiles of the HM1 flame, because of the presence of the inner vortex. The prediction at these locations is somewhat poor for both flames. Further downstream at the neck zone ($x/D > 1.3$), the agreement is good for the HM3 flame. It should be pointed out that a very good prediction of mixture fraction and mixture fraction variance is essential for proper evaluation of the combustion model. It is even more important for a CH_4/H_2 flame, because of its low stoichiometric mixture fraction value ($Z_{st} = 0.05$). A small error in mixture fraction or its variance will lead to a large error in calculation of temperature and species concentrations.

The comparison of the temperature profile is presented in Fig. 6. The agreement between the prediction and measurement for the HM1 flame is good up to $x/D < 1.3$. Further downstream, the temperature is overpredicted. It is worth mentioning that the significant overprediction at $x/D = 0.26$ is due to unusual lower experimental temperature rather than any shortcomings of the model. In this region,

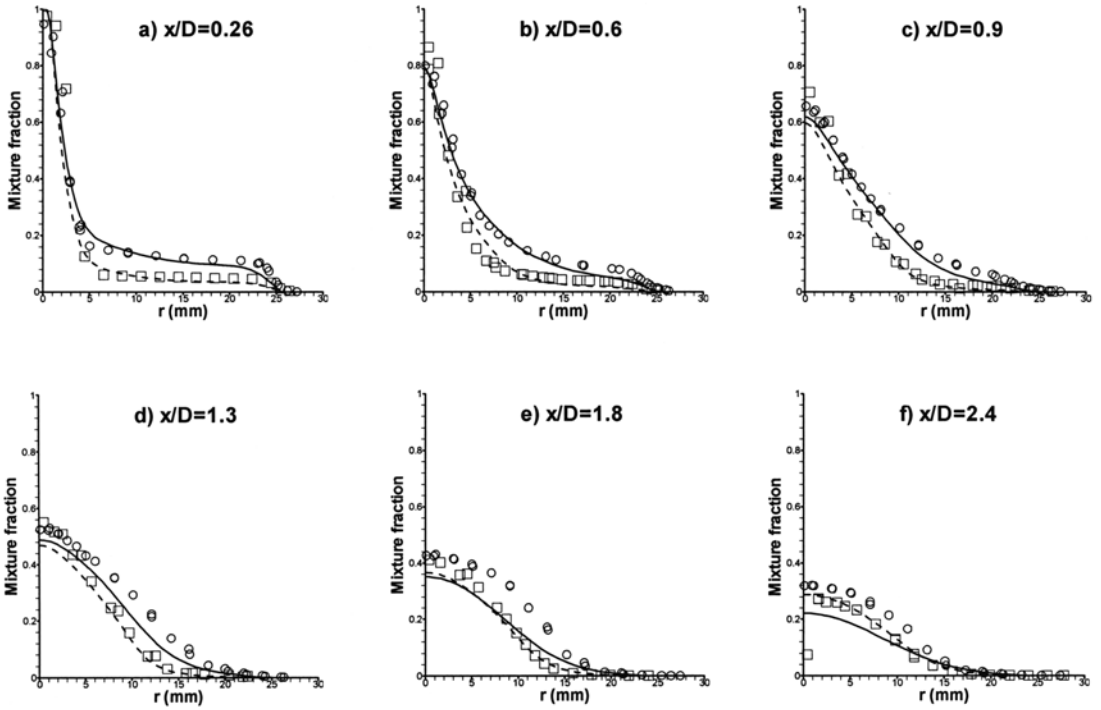

Fig. 4 Radial profiles of mixture fraction. ○ HM1 (measurement [19]); □ HM3 (measurement [19]); —— HM1 (prediction); - - - - HM3 (prediction)

intermittent local extinction was observed in the experiment leading to the lower temperature because of the averaging of the local extinguished and burned flames [**19**]. For the HM3 flame, the temperature is underpredicted at $x/D = 0.26$ and $x/D = 0.6$. This is because of the overprediction of the mixture fraction variance (see Fig. 5). The prediction is very good at $x/D = 0.9$. Further downstream in

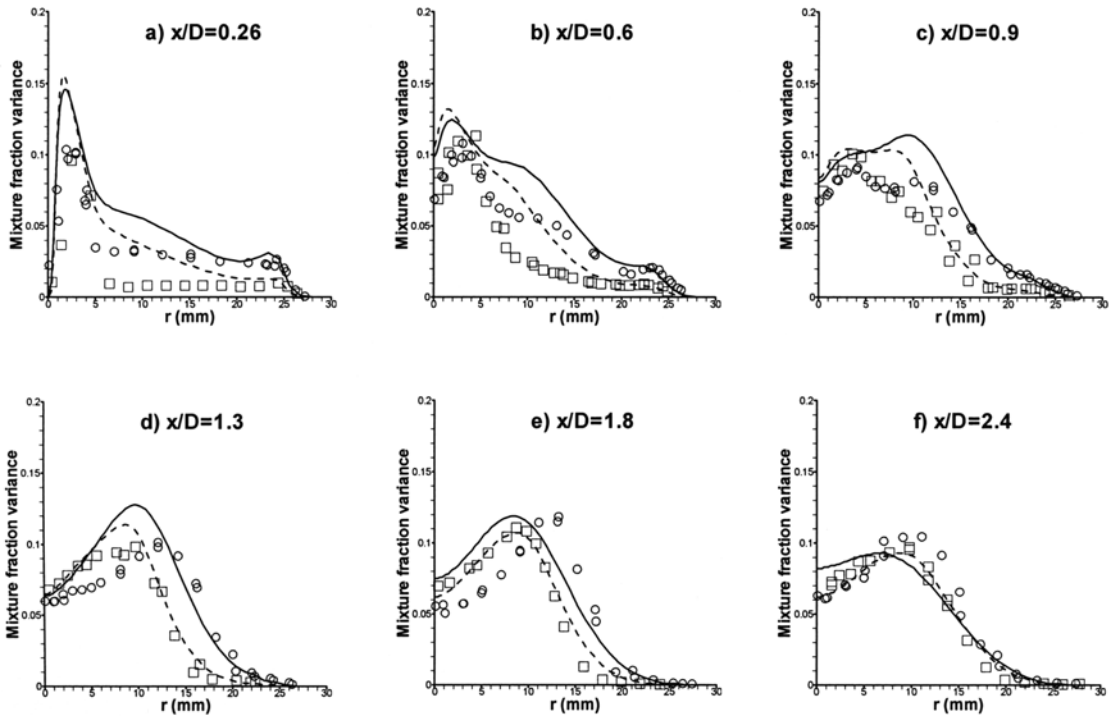

Fig. 5 Radial profiles of mixture fraction variance. ○ HM1 (measurement [19]); □ HM3 (measurement [19]); —— HM1 (prediction); - - - - HM3 (prediction)

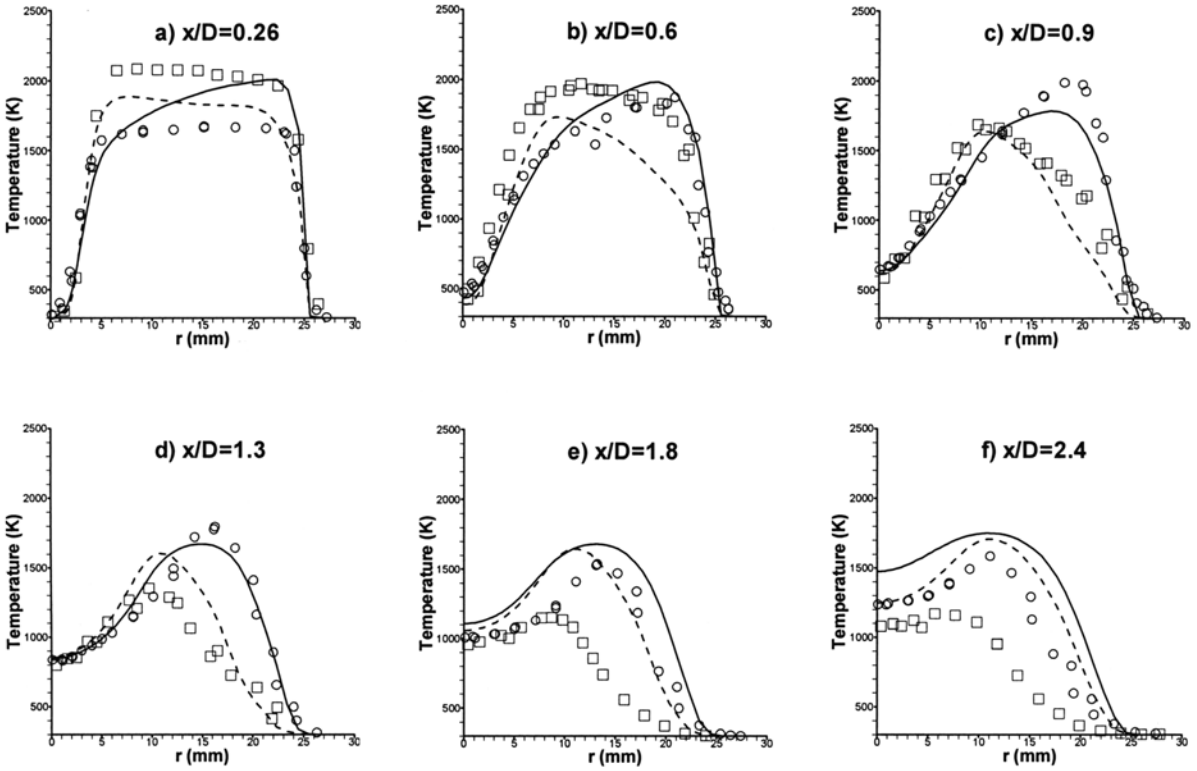

Fig. 6 Radial profiles of temperature. ○ HM1 (measurement [19]); □ HM3 (measurement [19]); —— HM1 (prediction); - - - - HM3 (prediction)

the neck zone, temperature is considerably overpredicted, though at these locations both the mixture fraction and mixture fraction variance are reasonably well predicted. This discrepancy can safely be attributed to the failure of the laminar flamelet model. The measurement shows considerable local extinction of the flame at the neck zone. Here the laminar flamelet model fails to predict the local extinction behaviour in the HM3 flame.

Radial profiles of mass fraction of H_2O and CO_2 are well reproduced for both flames as shown in Figs 7 and 8. The laminar flamelet model overpredicted H_2O and CO_2 in the neck zone in the HM3 flame, because of its failure to model the local extinction.

Radial mass fraction of OH is shown in Fig. 9. The OH is formed in a narrow zone inside the recirculation zone for the HM1 flame. The peak OH level gradually increases further downstream up to $x/D = 0.9$, and then starts decaying. The flamelet model predicts the narrow reaction zone, the gradual increase of the peak value, and the subsequent decay for the HM1 flame, reasonably well. The calculation, however, underpredicts the OH level inside the recirculation zone for the HM3 flame. This may be caused by the overprediction of the mixture fraction variance at these locations. At $x/D = 1.3$, the agreement between the experiment and measurement is good, as at this location both the mixture fraction and mixture fraction variance are well reproduced. At $x/D = 1.8$ and $x/D = 2.4$, the underprediction is caused by the failure of the laminar flamelet model to predict local extinction.

The classical laminar flamelet model was developed to handle the local extinction through the incorporation of an extinguished flamelet in the case the average scalar dissipation rate exceeding the extinction limit [**4**, **12**–**13**]. In the laminar flamelet library generation process, the scalar dissipation rate at which extinction occurs can be obtained by repeatedly increasing the scalar dissipation rate until the chemical reaction ceases. For the CH_4/H_2 fuel, the scalar dissipation rate at extinction is found to be 38.5/s from the one-dimensional laminar counterflow diffusion flame calculation. The calculated average scalar dissipation rate [from equation (8)] along the flame front of the HM1 and HM3 flames is shown in Fig. 10. The average scalar dissipation rate for the HM3 flame is higher than for the HM1 flame; however, the peak is much lower than the extinction limit. Despite this, the HM3 flame shows considerable local extinction, which the laminar flamelet model based on the average scalar dissipation rate failed to account for. The local extinction in the HM3 flame may be caused by the fluctuations in the scalar dissipation rate. Indeed, it has been found in experiment [**24**] and simulations [**25**, **26**] that the flame structure in a turbulent flame can be greatly influenced by fluctuations in the scalar dissipation

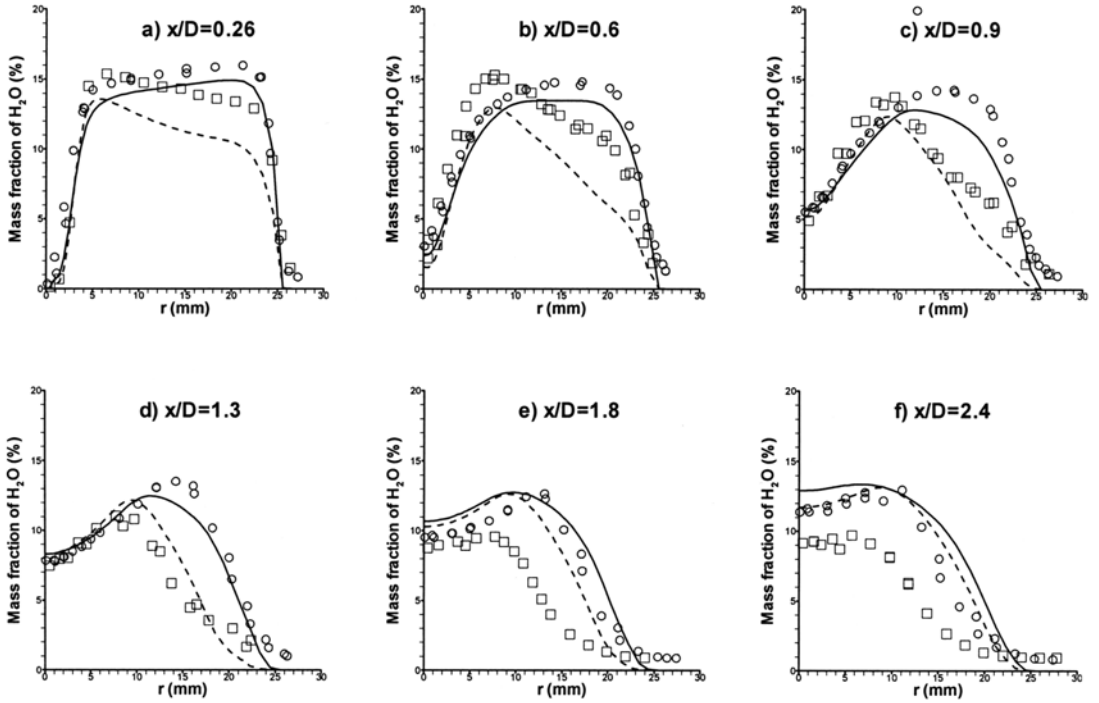

Fig. 7 Radial profiles of mass fraction of H_2O. ○ HM1 (measurement [19]); □ HM3 (measurement [19]); —— HM1 (prediction); - - - - HM3 (prediction)

rate. Consequently, it is entirely possible for the mean scalar dissipation rate to be smaller than the extinction limit, while the flame is quenched by the large fluctuations in the scalar dissipation rate over its limit [**26**]. It is, therefore, important to develop a model to include the influence of the fluctuating scalar dissipation rate using LES/DNS in order to handle the local extinction phenomenon.

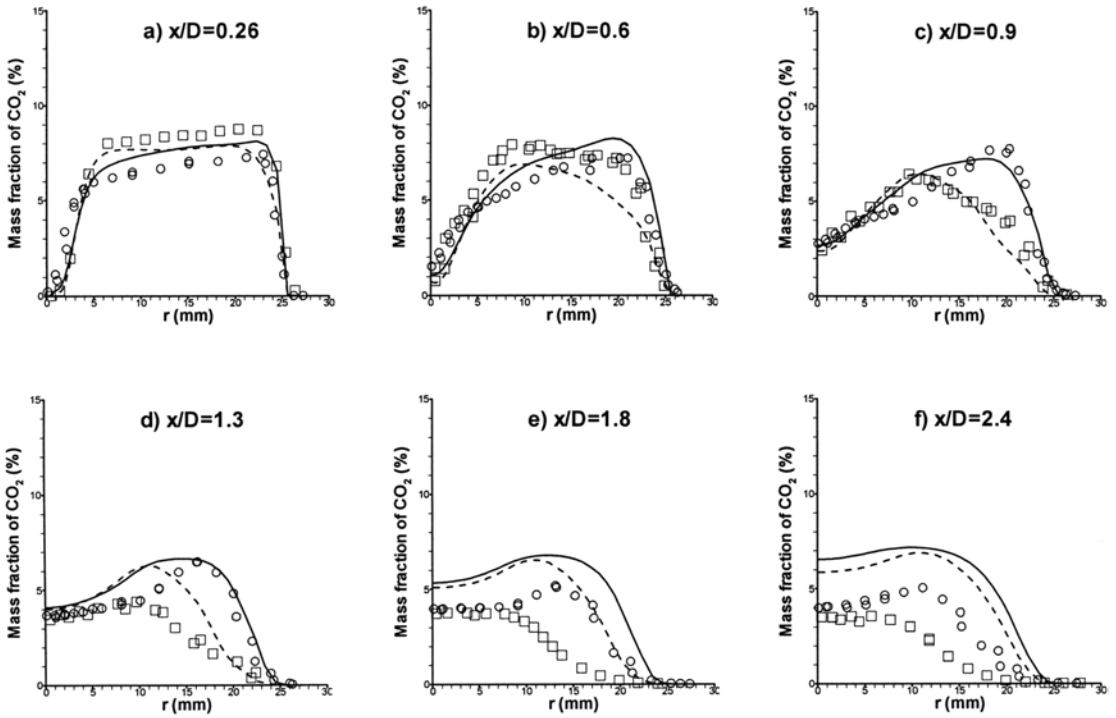

Fig. 8 Radial profiles of mass fraction of CO_2. ○ HM1 (measurement [19]); □ HM3 (measurement [19]); —— HM1 (prediction); - - - - HM3 (prediction)

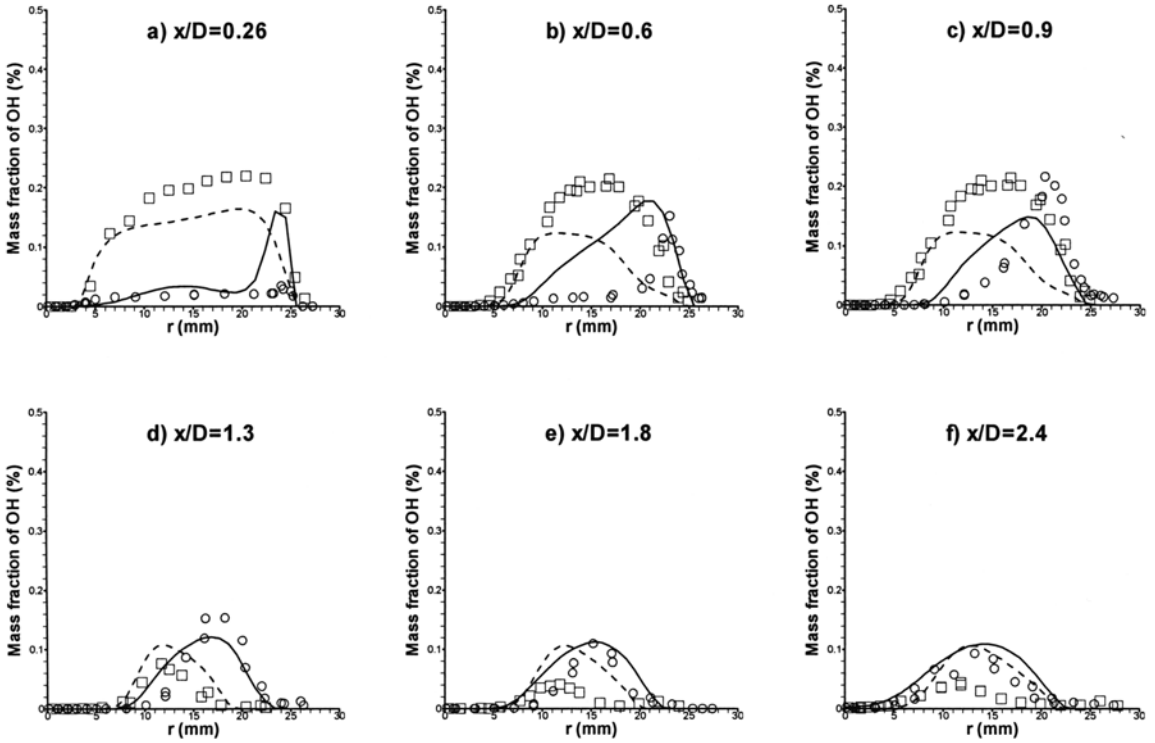

Fig. 9 Radial profiles of mass fraction of OH. ○ HM1 (measurement [19]); □ HM3 (measurement [19]); —— HM1 (prediction); - - - - HM3 (prediction)

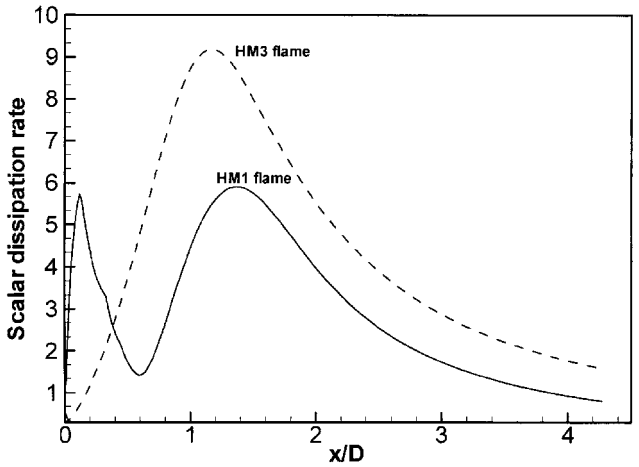

Fig. 10 Computed scalar dissipation rate along the flame front (along $Z = Z_{st} = 0.05$ line)

5 CONCLUSIONS

A numerical study of bluff-body stabilized flames using a laminar flamelet model is reported for different jet velocities. The effects of flow field on the structure of the flames are studied using a modified $k-\varepsilon$ turbulence model. Three different zones of bluff-body flame, (1) the recirculation zone, (2) the neck zone, and (3) the jet like zone are analysed using the numerical data. The importance of accurate prediction of the flow field before the evaluation of combustion model is also highlighted.

The temperature, mass fraction of H_2O, CO_2, and OH are well predicted for both the flames inside the recirculation zone. The small discrepancy observed between the flamelet calculation and measurements is due to the shortcomings of the turbulence model. At the neck zone, the prediction for the flame with lower velocity is also good. The laminar flamelet model has, however, failed to predict the local extinction effect at the neck zone in the flame with higher velocity.

REFERENCES

1 **Jones, W. P.** and **Whitelaw, J. H.** Calculations method for reacting turbulent flows: a review. *Combust. Flame*, 1982, **48**, 1–26.

2 **Magnussen, B. F.** and **Hjertager, B. H.** On modelling of turbulent combustion with special emphasis on soot formation and combustion. *Proc. Combust. Inst.*, 1976, **18**, 719–729.

3 **Gran, I. R.** and **Magnussen, B. F.** A numerical study of a bluff-body stabilised diffusion flame: Part 1 influence of turbulence modelling and boundary conditions. *Combust. Sci. and Technol.*, 1996, **119**, 171–190.

4 **Peters, N.** Laminar flamelet models in nonpremixed turbulent combustion. *Prog. Energ. Combust. Sci.*, 1984, **10**, 319–339.

5 **Peters, N.** Laminar flamelet concepts in turbulent combustion. *Proc. Combust. Inst.*, 1986, **21**, 1231–1250.
6 **Bilger, R. W.** Conditional moment closure for turbulent reacting flows. *Phys. Fluids A*, 1993, **5**(2), 436–444.
7 **Pope, S. B.** PDF methods for turbulent reactive flows. *Prog. Energ. Combust. Sci.*, 1985, **11**, 119–192.
8 **Pope, S. B.** Computations of turbulent combustion: progress and challenges. *Proc. Combust. Inst.*, 1990, **23**, 591–612.
9 **Bilger, R. W.** Future progress in turbulent combustion research. *Prog. Energ. Combust. Sci.*, 2000, **26**, 367–380.
10 **Coelho, P. J.** and **Peters, N.** Numerical simulation of a mild combustion burner. *Combust. Flame*, 2001, **124**, 503–518.
11 **Coelho, P. J.** and **Peters, N.** Unsteady modelling of a piloted methane/air flame based on the eulerian particle flamelet model. *Combust. Flame*, 2001, **124**, 444–465.
12 **Liew, S. K., Bray, K. N. C.,** and **Moss, J. B.** A stretched laminar flamelet model of turbulent nonpremixed combustion. *Combust. Flame*, 1984, **56**, 199–213.
13 **Gran, I. R., Melaaen, M. C.,** and **Magnussen, B. F.** Numerical simulation of local extinction effects in turbulent combustor flows of methane and air. *Proc. Combust. Inst.*, 1994, **25**, 1283–1291.
14 **Sanders, J. P. G.** and **Lamers, A. P. G. G.** Modeling and calculation of turbulent lifted diffusion flames. *Combust. Flame*, 1994, **96**, 22–23.
15 **Bray, K. N. C.** and **Peters, N.** Laminar flamelets in turbulent flames. In *Turbulent Reacting Flows* (Eds P. A. Libby and F. A. Williams) 1994, Ch. 2, pp. 63–113 (Academic Press, London).
16 **Hossain, M.** CFD modelling of turbulent nonpremixed combustion. PhD Thesis, Loughborough University, 1999.
17 **Hossain, M.** and **Malalasekera, W.** Modelling of a bluff body stabilised CH4/H2 flames based on a laminar flamelet model with emphasis on NO prediction. *Proc. Instn Mech. Engrs, Part A: J. Power and Energy*, 2003, **27**, 201–210.
18 **Hossain, M., Jones, J. C.,** and **Malalasekera, W.** Modelling of a bluff-body nonpremixed flame using a coupled radiation/flamelet combustion model. *Flow Turbul. Combust.*, 2001, **67**, 217–234.
19 **Dally, B. B., Masri, A. R., Barlow, R. S.,** and **Fiechtner, G. J.** Instanteneous and mean compositional structure of bluff-body stabilised nonpremixed flames. *Combust. Flame*, 1998, **114**, 119–148.
20 **Dally, B. B., Fletcher, D. F.,** and **Masri, A. R.** Flow and mixing fields if turbulent bluff-body jets and flames. *Combust. Theor. Model.*, 1998, **2**, 193–219.
21 **Rogg, B.** *RUN-1DL: 'The Laminar Flame and Flamelet Code'*, 1995.
22 **Bilger, R. W.** Structure of turbulent nonpremixed flames. *Proc. Combust. Inst.*, 1988, **22**, 475–488.
23 **Peters, N.** Flame calculations with reduced mechanisms-an outline. In *Reduced Kinetic Mechanisms for Applications in Combustion Systems* (Eds N. Peters and B. Rogg), 1993, Ch. 1, pp. 3–14 (Springer-Verlag, Berlin).
24 **Donbar, J. M., Driscoll, J. F.,** and **Carter, C. D.** Strain rates measured along the wrinkled flame contour within turbulent non-premixed jet flames. *Combust. Flame*, 2001, **125**, 1239–1257.
25 **Pitsch, H., Chen, M.,** and **Peters, N.** Unsteady flamelet modelling of turbulent hydrogen/air diffusion flame. *Proc. Combust. Inst.*, 1998, **27**, 1057–1064.
26 **Pitsch, H.** and **Steiner, H.** Scalar mixing and dissipation rate in large-eddy simulations of nonpremixed turbulent combustion, *Proc. Combust. Inst.*, 2000, **28**, 41–49.

APPENDIX

Notation

a	velocity gradient (strain rate)
C_{g1}, C_{g2}	model constant in the mixture fraction variance equation
$C_{\varepsilon 1}$, $C_{\varepsilon 2}$, C_μ	turbulence model constant
C_χ	constant in the scalar dissipation rate equation
D	diameter
G	turbulence production
k	turbulence kinetic energy
$P(\ )$	probability density function
u_j	velocity vector
x	axial location
x_i, x_j	distance vector
Z	mixture fraction
$\tilde{Z}''^2$	mixture fraction variance
ε	turbulent energy dissipation rate
μ_{eff}	effective viscosity
μ_t	turbulent viscosity
ρ	density
σ_k, σ_ε	turbulence model constant
σ_t	turbulent Prandtl number
σ_χ^2	standard deviation of the log-normal distribution
ϕ	scalar variables
χ	scalar dissipation rate

Superscripts

$\bar{}$	conventional ensemble average
$\tilde{}$	density-weighted ensemble average
$''$	density-weighted fluctuation